Laboratory Evidence for Stochastic Plasma-Wave Growth

D. R. Austin,[1,2] M. J. Hole,[1,3] P. A. Robinson,[1] Iver H. Cairns,[1] and R. Dallaqua[4]

[1]*School of Physics, University of Sydney, New South Wales, 2006, Australia*
[2]*Clarendon Laboratory, University of Oxford, Oxford OX1 3PU, United Kingdom*
[3]*Research School of Physical Sciences and Engineering, The Australian National University, Australian Capital Territory, 0200, Australia*
[4]*Laboratório Associado de Plasma-LAP, Instituto Nacional de Pesquisas Espaciais-INPE/MCT, CP 515, 12201-970, São José dos Campos, SP, Brazil*

(Received 1 November 2006; published 14 November 2007)

The first laboratory confirmation of stochastic growth theory is reported. Floating potential fluctuations are measured in a vacuum arc centrifuge using a Langmuir probe. Statistical analysis of the energy density reveals a lognormal distribution over roughly 2 orders of magnitude, with a high-field nonlinear cutoff whose spatial dependence is consistent with the predicted eigenmode profile. These results are consistent with stochastic growth and nonlinear saturation of a spatially extended eigenmode, the first evidence for stochastic growth of an extended structure.

DOI: 10.1103/PhysRevLett.99.205004 PACS numbers: 52.25.Gj, 52.35.Qz, 52.80.Mg

Statistical plasma theories, such as stochastic growth theory [1,2] (SGT) and self-organized criticality (SOC) [3,4], have enjoyed wide success in describing nonuniform fluctuations in complex systems. In particular, complex initial and/or boundary conditions, sources, and sinks of energy, and nonlinear evolution can lead to a highly nonuniform plasma structure in a state of dynamical equilibrium. In these systems, textbook models of wave growth that assume simply structured initial conditions offer little insight into emergent properties such as marginal stability. In contrast, statistical plasma theories connect the salient features of the wave physics to characteristic distributions of wave properties. For example, in SGT a randomly varying wave growth rate leads to a lognormal distribution, in SOC ''sandpile avalanche'' type behavior yields scale-free power-law distributions, while Gaussians are expected in many contexts. SGT has wide applicability [5,6] including type III solar radio bursts [5], magnetospheric Langmuir, beam and z-mode waves [7], and pulsar emissions [8], plus a range of quasilinear, particle-in-cell, and other simulations [6]. Evidence for other statistical plasma theories, such as SOC, has been found in solar flares and the intermittent turbulence of the Earth's magnetotail [9–11] and it has been invoked to describe confinement and transport phenomena in magnetically confined plasmas [12,13].

These successes motivate searching for new applications of statistical plasma theories. In this Letter we perform a statistical analysis of fluctuations in a laboratory plasma and find lognormal distributions over a wide range of field strength, the first laboratory evidence for an SGT state. Also, a departure from lognormality at high-field strengths is shown to be consistent with nonlinear saturation of a spatially extended eigenmode structure.

The device used to obtain the data is a vacuum arc centrifuge (VAC), a magnetized plasma device originally designed to separate nuclear isotopes. It uses an arc discharge to form a multiply ionized ($Z > 1$) low temperature ($T \approx 6 \times 10^4$ K) high density ($n_i \approx 10^{18}$ m^{-3}) Mg plasma. The plasma is situated in an axial magnetic field ($B = 0.1$ T) and is formed by drawing a 1 kA arc between a metal cathode and a wire mesh anode 60 mm distant. As the return current passes through the mesh, resistive losses generate a radial electric field. The interaction of the resultant radial current with the axial magnetic field drives the plasma into rigid rotation at approximately 30 kHz. The plasma then streams supersonically through the mesh with axial velocity $\approx$10 kms^{-1} and is confined by the axial

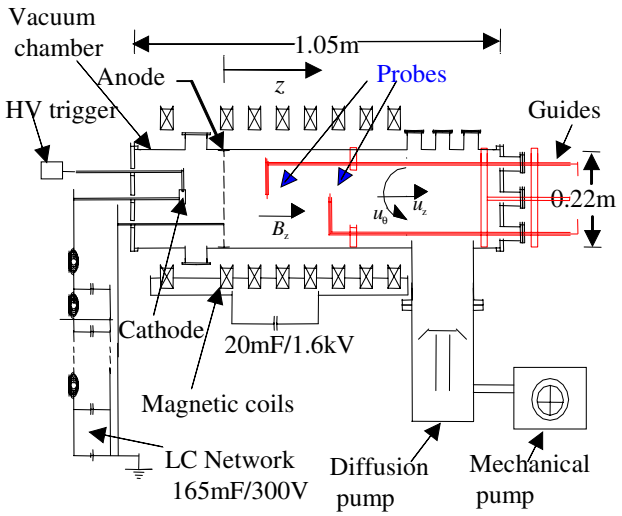

FIG. 1 (color online). Schematic of the plasma centrifuge. The cathode is vaporized by the high voltage trigger and accelerated towards the anode mesh by an arc discharge. The combination of radial motion and axial magnetic field sets the plasma into rotation, and it streams helically through the anode to the end plate. Adapted from Ref. [15].

magnetic field. Figure 1 shows a schematic of the VAC used here, the Plasma Centrifuge at the Laboratório Associado de Plasma of Brazil's Instituto Nacional de Pesquisas Espaciais [14].

Data for this work are from an extensive set of experiments designed to explore properties of the electrostatic oscillations observed in VACs [15]. A Langmuir probe was inserted 150 mm downstream of the anode mesh to measure the floating potential. Measurements were taken at nine radial locations from $r = 0$ mm to $r = 32.5$ mm. At each location, eight plasma discharges were recorded. The floating potentials were sampled at 10^6 samples per second over a 5 ms interval (during which the discharge current was flattopped) commencing 5 ms into the 16 ms pulse-length discharge. The resulting 72 discharges yielded the data analyzed below. Figure 2(a) shows the power spectrum of data from one discharge at $r = 10$ mm, along with the power spectrum averaged over all discharges at that position. The most striking feature is a 28 kHz quasiperiodic oscillation, modulated by a slowly varying envelope, whose -3 dB bandwidth is ≈ 10 kHz. By comparing field profiles with a linear analysis based on a steady state model in rigid body motion, the oscillation was identified as a density gradient driven drift wave [15], propagating axially and azimuthally. The azimuthal velocity was approximately the same as that of the plasma rotation. The linear analysis predicted a growth time constant of only $\approx 0.1\%$ of the plasma lifetime, strongly suggesting the occurrence of nonlinear saturation and consistent with the observation of second and third harmonics seen in Fig. 2(a). To confirm the presence of nonlinear interaction, we computed the bicoherence spectrum [16], defined at frequencies f_1 and f_2 of the probe voltage V by $B(f_1, f_2) = \langle V(f_1)V(f_2)V^*(f_1 + f_2)\rangle$ (with suitable normalization), where the asterisk denotes complex conjugation and angle brackets denote averaging over an ensemble of sample Fourier-transformed time series of V. Here, we split the data from each shot into segments of 512 samples each (with 50% overlap between segments), computed the Fourier transform of each segment, and then the bicoherence of each shot by averaging over the segments. In the bicoherence, nonlinear interactions between Fourier components at f_1 and f_2 produce correlated phases, resulting in high $B(f_1, f_2)$. A representative bicoherence, averaged over the eight shots at $r = 10$ mm, is shown in Fig. 3. Nonlinear interactions between components at 28 kHz are revealed, an indication of frequency doubling processes. Other strong interactions include sum-frequency generation between the first and second harmonic, which yields the peak at (28, 56) kHz, and frequency doubling of the second harmonic, corresponding to the (56, 56) kHz peak.

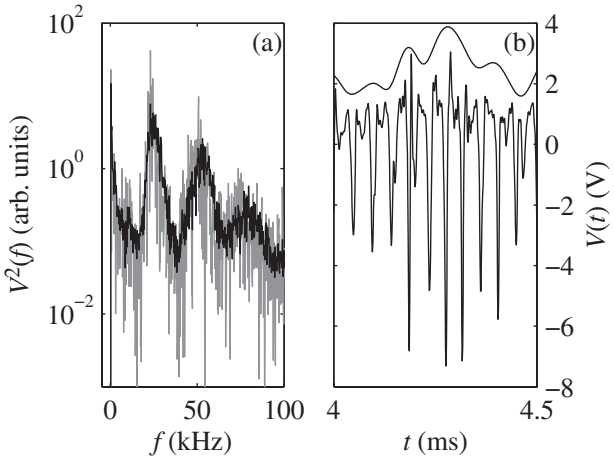

FIG. 2. (a) Floating potential at $r = 10$ mm: power spectrum of a single shot (gray) and average power spectrum over eight shots (solid). (b) Floating potential fluctuation (lower curve) and corresponding combined harmonic amplitude V_E given by Eq. (1) (upper curve).

To investigate the statistical properties of the field, we computed the wave energy density $W(t)$ as follows: the slowly varying mean floating potential was removed by high-pass filtering with a cutoff at $f_C = 20$ kHz. After low-pass filtering at 167 kHz (one-third the Nyquist frequency), the resulting signal was squared, causing sum and difference frequencies to be generated between the various harmonics. By low-pass filtering with cutoff $f_E = 15$ kHz, we obtained, up to an undetermined proportionality, the baseband energy density

$$W(t) \propto V_R^2(t) = V_1^2(t) + V_2^2(t) + V_3^2(t), \qquad (1)$$

where $V_i(t)$ is the ith harmonic amplitude and $V_R^2(t)$ is the combined intensity of all harmonics. All filtering was performed in the frequency domain and filters had an error-function roll-off of characteristic width 5 kHz. Figure 2(b) shows the time series after the initial high-pass filtering step, along with the combined harmonic amplitude $V_R(t)$. The latter does not follow the field envelope exactly, since it is a slowly varying phase-independent estimate of the total energy in all three harmonics, whereas the instantaneous amplitude is a coherent superposition of the harmonics and depends on their relative phases. We

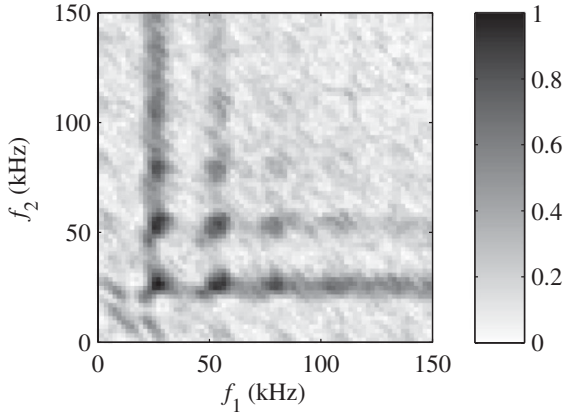

FIG. 3. Amplitude of the bicoherence, defined in the text, after averaging over the eight shots at $r = 10$ mm.

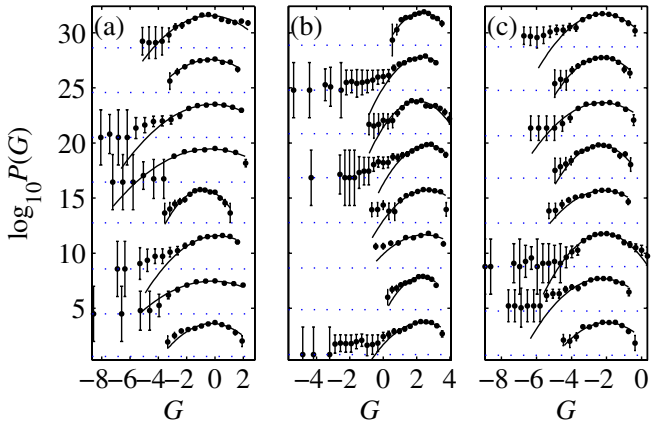

FIG. 4 (color online). Probability distribution functions of field-strength gain at (a) $r = 0$ mm, (b) $r = 10$ mm, and (c) $r = 32.5$ mm, normal distribution fits (solid line) and one-bin count level (dotted line); at each radial position, results from the eight discharges are shown with differing vertical offsets for clarity. Error bars are ± 1 standard deviation.

have confirmed that, if only one harmonic is present, V_R reproduces the field envelope. Inclusion of all three nonlinearly interacting harmonics in $W(t)$ was necessary for the good agreement with SGT shown below.

To enable comparison with SGT the gain $G = \log_e W$ was binned, with representative results shown in Fig. 4. Good agreement with fitted normal distributions is seen over a range $\Delta G \approx 5$, or two decades in W. This is consistent with SGT, which predicts lognormal distributions of wave energy density and hence normal distributions of G. Some shot-to-shot variation is also visible, especially at low-field strengths, which we attribute to the complex dynamics of the arc discharge, which are not perfectly replicated in each shot. The elevated low-field tail of the distribution seen in Fig. 4 is due to the approach to the one count per bin statistical limit, while the drop-off at high fields suggests the onset of nonlinear saturation, consistent with the above observation of a phase-correlated second harmonic via the bicoherence. We modified our fitting function to incorporate both effects. Nonlinear saturation can be included in SGT by adding an absorbing boundary using the method of images [2]. This involves one additional parameter, the nonlinear cutoff level G_C such that $P(G) = 0$ for $G > G_C$. A first approximation of the effect of low bin counts is to add a constant $\epsilon \propto 1/(N\Delta)$, where N is the number of samples and Δ the bin width, so that ϵ corresponds to one sample per bin. The resulting distribution is

$$P(G) = \epsilon + A\left\{\exp\left[\frac{-(G-\mu_G)^2}{2\sigma_G^2}\right] - \exp\left[\frac{-(2G_C-\mu_G-G)^2}{2\sigma_G^2}\right]\right\}, \quad (2)$$

where G_C is the nonlinear cutoff level and A is a normalization constant. Figure 5 shows $P(G)$ averaged over each discharge at for various r, fitted to the resulting distribution (2). Where the error bars are small, and the data are statistically significant, agreement with the prediction of SGT in the presence of a nonlinear cutoff is excellent. In the low probability tail, where the predicted distribution and data approach the one-count per bin level, there is also agreement but this is inconclusive due to the large errors and the rough approximation made above to the effects of the one-count level. This approximation is also likely the cause of the poor agreement in the crossover from good statistics to the one-count level. Since the disagreement occurs only where statistics are poor, and is excellent where they are good (reduced $\chi^2 < 1$ for points no more than $\Delta G = 3$ below the peaks of the curves in Fig. 5), it does not appear to be critical to the overall interpretation. Its full resolution will require detailed modeling of the low-field structure and statistics, including the effects of noise, which is beyond the scope of this Letter. However, the level at which the discrepancy occurs is consistent with noise levels observed, a point discussed further below.

Systematic radial dependence of G_C and μ_G is evident in Fig. 5, with the highest values occurring at $r = 10$ mm. This motivates comparison with the theoretical eigenmode potential $V_{\text{th}}(r)$ [15]. The finite spatial resolution of the measurements, primarily determined by the Langmuir probe radial extent of 2 mm, was accounted for by convolving $V_{\text{th}}(r)$ with a Gaussian kernel function $K(r)$ of corresponding width. Since the theoretical gain was only determined up to an arbitrary additive constant G_0, this was a free parameter which we determined by fitting. A further refinement here was the inclusion of a spatially uniform background energy density F (discussed shortly) as an additional fit parameter, so the fitted function is

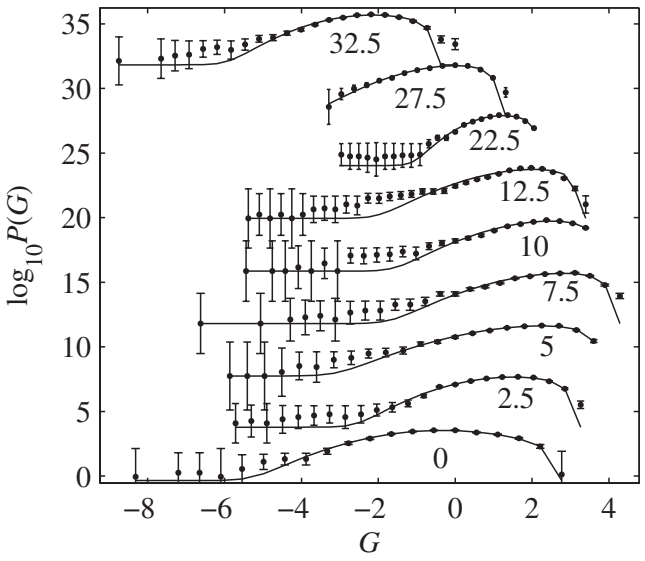

FIG. 5. Distributions $P(G)$ with best fit to SGT including a one sample per bin background and nonlinear cutoff, labeled by radial position in millimeters. For clarity, plots are vertically offset with spacing 4. Error bars are ± 1 standard deviation.

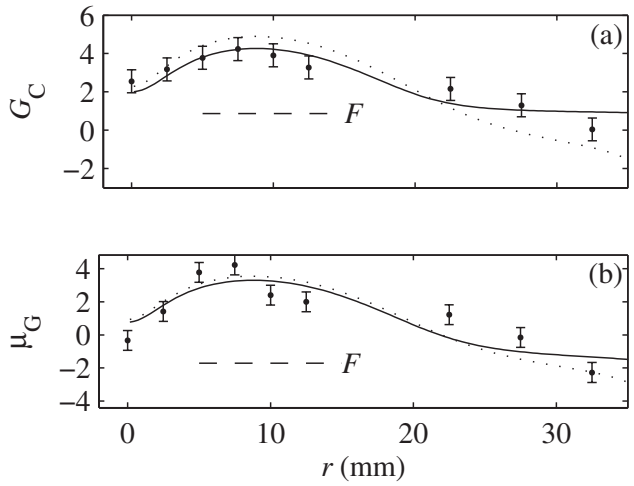

FIG. 6. Gain vs r; (a) nonlinear cutoff G_C, as extracted from gain PDFs (data points), and fitted theoretical curve (3) with (solid line) and without (dotted line) background field F; (b) stochastic mean μ_G (data points), and fitted theoretical curve with (solid line) and without (dotted line) background field. Error bars are ± 1 standard deviation. The level of the spatially uniform background field F is also shown (dashed).

$$G_{\text{fit}} = G_0 + \log_e[\{V_{\text{th}}(r) * K(r)\}^2 + F], \qquad (3)$$

where $*$ denotes spatial convolution. Equation (3) was fitted to both μ_G and G_C independently, with the results shown in Fig. 6. Uncertainties in μ_G and G_C were estimated from the shot-to-shot variation. The dotted curves show the fitted Eq. (3) with $F = 0$, and show reasonable agreement with the stochastic parameters. Allowing F to vary (solid curves) improves the fits considerably, particularly at large r. We attribute F to noise (seen over the full frequency spectrum in Fig. 2) and/or the presence of higher order modes which concentrate energy near the edges of the plasma stream, for which there is some evidence in the form of higher bicoherence in analogs of Fig. 3 at larger r. For both μ_G and G_C the fitted F is only about 1% of the level of the peak of the theoretical curve peak at $r = 9$ mm, a value that suggests that these background fields may also cause the poor fits at $\Delta G = 3$–5 below the peaks in Fig. 5. The good agreement between the fitted and predicted nonlinear cutoff G_c, shown in Fig. 6(a), and stochastic growth mean μ_G, shown in Fig. 6(b), thus indicates that the entire eigenmode structure is undergoing stochastic growth and nonlinear saturation, the first detection of stochastic growth of an extended structure.

Although one cannot consider all conceivable alternatives to a lognormal, it is worth noting that the results here are certainly not compatible with Gaussian distributions of W, even if nonlinear and background-field effects were allowed for, since Gaussians fall off too quickly far from the peak. Likewise, there is no sign of the scale-free power-law distributions of wave intensity that might be expected if SOC applied, a point further reinforced by the eigenmode structure setting a preferred scale.

In summary, we have shown that fluctuation eigenmodes in a vacuum arc centrifuge have a field-strength distribution that is consistent with a lognormal, modified by nonlinear saturation at high-field strengths and noise effects at low ones, and with a spatial structure that follows the predicted eigenmode profile. These results strongly imply that the waves are undergoing stochastic growth. This represents the first laboratory confirmation of SGT and the first evidence for stochastic growth of a spatially extended eigenmode. Given these results and the numerous situations where SGT is relevant, as cited in the introductory paragraphs, further investigation of statistical plasma theories (not only SGT) in other experimental settings is thus warranted.

The Australian Research Council supported this work.

[1] P. A. Robinson, Sol. Phys. **139**, 147 (1992).
[2] P. A. Robinson, Phys. Plasmas **2**, 1466 (1995).
[3] P. Bak, C. Tang, and K. Wiesenfeld, Phys. Rev. Lett. **59**, 381 (1987).
[4] R. O. Dendy and P. Helander, Phys. Rev. E **57**, 3641 (1998).
[5] P. A. Robinson, I. H. Cairns, and D. A. Gurnett, Astrophys. J. **407**, 790 (1993).
[6] P. A. Robinson, B. Li, and I. H. Cairns, Phys. Rev. Lett. **93**, 235003 (2004).
[7] I. H. Cairns and P. A. Robinson, Phys. Rev. Lett. **82**, 3066 (1999).
[8] I. H. Cairns, S. Johnston, and P. Das, Astrophys. J. **563**, L65 (2001).
[9] E. Lu and R. Hamilton, Astrophys. J. **380**, L89 (1991).
[10] S. Chapman, N. Watkins, R. Dendy, P. Helander, and G. Rowlands, Geophys. Res. Lett. **25**, 2397 (1998).
[11] A. Lui, S. Chapman, K. Liou, P. Newell, C. Meng, M. Brittnacher, and G. Parks, Geophys. Res. Lett. **27**, 911 (2000).
[12] D. Newman, B. Carreras, P. Diamond, and T. Hahm, Phys. Plasmas **3**, 1858 (1996).
[13] S. C. Chapman, R. O. Dendy, and B. Hnat, Phys. Rev. Lett. **86**, 2814 (2001).
[14] E. D. Bosco, S. W. Simpson, R. S. Dallaqua, and A. Montes, J. Phys. D **24**, 2008 (1991).
[15] M. J. Hole, R. S. Dallaqua, S. W. Simpson, and E. Del Bosco, Phys. Rev. E **65**, 046409 (2002).
[16] Y. C. Kim and E. J. Powers, IEEE Trans. Plasma Sci. **7**, 120 (1979).